Journal of Hazardous Materials 215–216 (2012) 166–172

Contents lists available at SciVerse ScienceDirect

Journal of Hazardous Materials

journal homepage: www.elsevier.com/locate/jhazmat

Preparation of ZnO/SiO_2 gel composites and their performance of H_2S removal at room temperature

Guoqiang Liu[a], Zheng-Hong Huang[a,*], Feiyu Kang[a,b]

[a] Laboratory of Advanced Materials, Department of Materials Science and Engineering, Tsinghua University, Beijing 100084, China
[b] Institute of Advanced Materials Research, Graduate School at Shenzhen, Tsinghua University, Shenzhen 518055, China

ARTICLE INFO

Article history:
Received 11 October 2011
Received in revised form 14 January 2012
Accepted 18 February 2012
Available online 24 February 2012

Keywords:
Silica
Zinc oxide
Gel composite
Hydrogen sulfide
Desulphurization

ABSTRACT

ZnO/SiO_2 gel composites with different active component loading were prepared by sol–gel method combined with ambient drying process, followed by thermal treatment. The gel composites were characterized by scanning electron microscopy (SEM), nitrogen adsorption, X-ray diffraction (XRD), FTIR and X-ray photoelectron spectroscopy (XPS), and their performances for H_2S removal were evaluated by dynamic testing at room temperature. The as prepared materials exhibited high surface area with multimodal pore size distributions in micropore and mesopore region. The porous properties were significantly influenced both by the ZnO loading ratio and the treated temperature. The gel composites showed a high performance for H_2S removal, with the highest H_2S adsorption capacity of 96.4 mg/g for the sample treated at 400 °C with 30 wt% ZnO. Both physisorption and the active phase reactivation governed the H_2S removal process. It needs to optimize the composites' porous structure and active component loading amount.

1. Introduction

A significant quantity of H_2S is generated in many industrial processes, and it is necessary to decrease the H_2S concentration down to an allowable value since they are extremely malodorous and toxic, being as the sources of acid rain, causing pipeline corrosion and limiting plant lifetime [1]. In addition, more stringent environmental regulations call for more efficient and economical ways to remove sulfur-containing species from liquid or gaseous phases to minimize the formation of environmentally toxic species. Thus, the removal of H_2S at low temperature attracts much more attention.

Scrubbing, adsorption and biological treatment are main conventional methods for H_2S removal in commercial processes [2]. Currently, one of the most important topics on the removal of H_2S is the method that adsorption of H_2S on various porous materials such as activated carbons (ACs) [3], modified ACs [4,5], activated carbon films [6] and modified clay [7], etc. Various drawbacks of these materials have been concluded by Wang et al. [8], who proposed to use ordered mesoporous material such as SBA-15 to develop novel solid catalysts for the applications of H_2S gas purification.

Because the H_2S adsorption performance of the adsorbents depends on their porosity and surface chemistry, it is an interesting route to improve desulphurization capacity by introducing active phase such as various metal oxides into mesoporous materials. Due to its high equilibrium constant for sulfidation and thermal stability of sorbents and their sulfides, ZnO and Zn-based sorbents are very attractive for the removal of H_2S at low temperature. Garces et al. [9] investigated the desulfurization performance at low temperatures (60–400 °C) of a commercially available ZnO, and found that the sorbent's sorption capacity at breakthrough increased with the sulfidation temperature, reaching 87% of the theoretical value for desulfurization at 400 °C. Various Zn–Ti-based mixed metal oxides were prepared by the sol–gel method, and their adsorption towards H_2S from a gas mixture of H_2S, H_2, CO and H_2O was studied in the range of 25–100 °C [10]. The effects of the chemical nature and atom ratio in the composites of a third metal additive (M = Mn, Cu, Mo) in the M–Zn–Ti–O solid on the H_2S adsorption and regeneration performance were also studied. The sulfur uptake capacity at 25 °C of Fe- and Mn-promoted sorbents Fe_x–Mn_y–$Zn_{1-x-y}O/SiO_2$ significantly exceeded that of both commercial unsupported ZnO sorbents and un-promoted supported ZnO/SiO_2 sorbents, and sulfur capacity and breakthrough characteristics remained satisfactory after multiple (~10) cycles of adsorption/regeneration, with regeneration performed by a simple and robust heating in air [11]. Yang and Tatarchuk [12] also investigated the desulfurization performance of transition metal doped ZnO/SiO_2 at low temperature, and found that copper-doped sorbent Cu-ZnO/SiO_2 demonstrated much higher saturation sulfur

* Corresponding author. Tel.: +86 10 62773752; fax: +86 10 62771160.
E-mail address: zhhuang@tsinghua.edu.cn (Z.-H. Huang).

0304-3894/$ – see front matter © 2012 Elsevier B.V. All rights reserved.
doi:10.1016/j.jhazmat.2012.02.050

capacity than ZnO/SiO_2 in a wide temperature range of 20–400 °C, and can be easily regenerated in air at low temperature. ZnO is also usually used to functionalize SBA-15 as an efficient active phase, and the as-prepared materials show high H_2S adsorption capacity, which attributed to the integration of the pore structure of mesoporous material and the promising desulphurization properties of ZnO nanoparticles [8,13]. However, the synthesis of SBA-15 needs a large amount of HCl solution and takes long time. Besides, the dispersion of metal oxides in support materials such as silica gel, SBA-15, activated carbons, etc. is not very satisfying by using wet impregnation method, and it is also difficult to get accurate information of ratio metal oxides deposited in SBA-15. Therefore, it is of significance to select a kind of mesoporous material which is easy to prepare, and find an efficient method to deposit metal oxides in the support materials.

The sol–gel process allows elaborating the solid material from a solution by using sol or gel as an intermediate step, which involves wet chemistry reactions and sol–gel chemistry based on the transformation of molecular precursors into an oxide network by hydrolysis and condensation reactions [14]. Silica gel is typical sol–gel-derived mesoporous materials, which are extremely fascinating as well as very promising for a large number of applications due to their nanostructured and porosity. Various metal oxides such as ZnO [15], CuO [16] and Fe_2O_3 [17] also have been prepared by sol–gel process. Therefore, a synthesis route that mixing the sols of metal oxide and silica to obtain highly porous gel composites would improve the dispersion of active phase in support material. In the present study, silica sol and ZnO sol were synthesized respectively, and ZnO/SiO_2 gel composites with different weight ratio of ZnO were prepared by mixing the sols followed by gelation process. The mesoporous gel composites were characterized by various methods, and H_2S desulphurization performance was also investigated. The factors that have influence on porosity of the gel composites and H_2S removal performance were discussed.

2. Experimental

2.1. Synthesis of ZnO/SiO_2 gel composites

The silica alcosol was prepared by mixing tetraethylorthosilicate (TEOS), anhydrous ethanol (EtOH), distilled water and hydrochloric acid in a 250 mL beaker at a molar ratio of $1:6:4:10^{-3}$ and stirring for 30 min, in which hydrochloric acid was used as an acid catalyst for the hydrolysis of TEOS. The starting materials used to synthesize ZnO alcosol were zinc acetate dihydrate ($Zn(CH_3COO)_2{\cdot}2H_2O$), monoethanolamine (MEA) and EtOH. MEA was dissolved in EtOH in a concentration of 1.0 mol/L and stirred for 20 min, and then $Zn(CH_3COO)_2{\cdot}2H_2O$ was added. The molar ratio of [MEA]: [Zn^{2+}] was 1.5:1. The solution was stirred with reflux at 20 °C for 1 h, and aged for 24 h after filtering before a homogeneous transparent colloid was obtained. All of the reactants used in the experiments were of analytical reagent purity.

Two series of ZnO/SiO_2 gel composites were prepared by adding ZnO alcosol in the SiO_2 alcosol followed by thermal treatment at different temperatures. The sol mixture was stirred for 15 min, and then kept for gelation. After gelation, the alcogel was immersed in excess of EtOH at room temperature and maintained for one day, and then the alcogel was dried at 80 °C for 2 h. Assuming a complete hydrolysis and condensation of the Zn(II) salt into ZnO, samples with the weight ratios for $ZnO/(ZnO + SiO_2)$ of 5, 10, 20, 30, 40 and 50%, treated at 500 °C for 3 h were obtained. The samples with 30 wt% ZnO component calcined at 200–600 °C for 3 h were also prepared. All samples are named as SZ*x*-*y*, in which *x* denotes the ZnO weight ratio in %, and y denotes the treating temperature in °C. Sample after desulphurization experiment is named as SZ*x*-*y*-E.

2.2. Characterization of materials

The porous structures of the samples were studied by adsorption of N_2 at −196 °C with automatic instrument (Belsorp max) over a wide relative pressure range from about 10^{-6} to 0.998. Prior to the measurements, all samples were degassed at 200 °C for 12 h to ensure that the samples were clean and free of moisture. The specific surface area of the samples was assessed by the standard Brunauer–Emmett–Teller (BET) method, and the pore size distributions (PSDs) were calculated by using the Density Functional Theory (DFT). Mid-IR spectra (4000–500 cm^{-1}) were collected on a Nicolet 560 FT-IR spectrometer using pellets with samples dispersed in KBr. X-ray diffraction (XRD) analyses were carried out by using X-ray diffractometer (Rigaku D/max-2500) with Cu-Kα (40 kV, 40 kA) radiation. The data were recorded over a 2θ range of 5–90°. The morphologies of samples were observed by a LEO1530 (LEO, Oberkochen, Germany) field emission scanning electron microscopy (SEM). Energy dispersive X-ray (EDX) analysis was performed in an EDAX (Model 6498, Oxford Instruments, England). Gold was used as conductive material for samples coating. X-ray photoelectron spectroscopy (XPS) was carried out by using an X-ray photoelectron spectrometer (ESCALAB250Xi, ThermoFisher) with Al Kα radiation to obtain the information on surface atomic concentration and oxidation state, and the binding energies were calibrated by the carbon (C1s = 284.8 eV). The spectra obtained were curve-fitted with the nonlinear least-square iterative technique based on the Gaussian function after baseline subtraction using Shirley's method.

2.3. Desulphurization test

The performance of samples for H_2S removal was evaluated at ambient conditions (20 °C, 1 atm) by the breakthrough capacity test system, as shown in Fig. 1. The adsorbent was packed into a glass column (length of 250 mm, diameter of 6 mm). The inlet concentration of H_2S (balance of N_2) was 100 ppm and the flow rate was 300 mL/min. The inlet and out-let gas (H_2S) was analyzed by gas chromatograph (Shimadzu, GC2014) equipped with a flame photometry detector (FPD). All outlet gases from the reactor were sampled with an online auto-sampling system and analyzed every 3 min. The breakthrough time was defined as the time from the beginning of the desulfurization to the time when the H_2S concentration at the outlet reached 1 ppm. The H_2S breakthrough capacity in terms of milligrams of H_2S per gram of material was calculated by integration of the area above the breakthrough curve and from the H_2S concentration in the inlet gas, the flow rate, the breakthrough time, and the mass of material.

Regeneration of the "sulfided" sorbents was performed in a furnace at 400 °C in air for 3 h, which was the same as the gel composite that was prepared. Before any H_2S adsorption measurements were taken, the materials were always pretreated at this condition.

3. Results and discussions

3.1. Morphology and nitrogen adsorption

Fig. 2 shows the scanning electron micrographs of silica xerogel, ZnO/SiO_2 gel composites before and after desulphurization. All samples comprise interconnected primary silica or ZnO/SiO_2 particles to form a three-dimensional (3D) nanoporous structure. These samples exhibit relatively denser network with small pores and also good interconnectivity between silica or ZnO/SiO_2 chains. The microstructure of samples comprises irregular-shaped clusters with loose packing and also wide separation between the chains. This is due to the fact that the

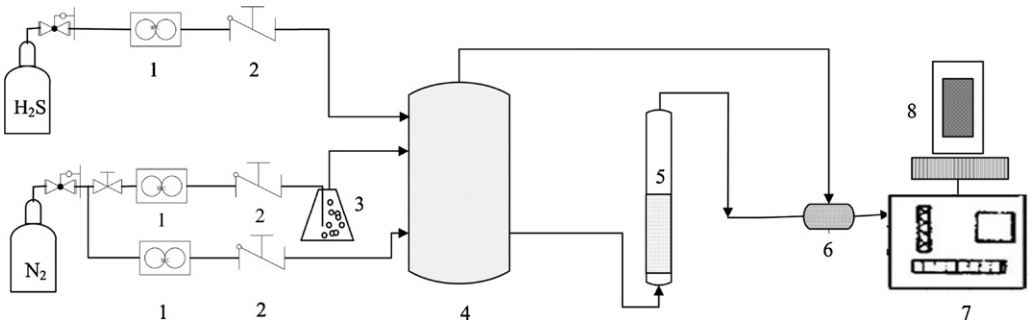

Fig. 1. Schematic representation of H_2S breakthrough testing system: (1) Mass flow controller; (2) one-way valve; (3) isothermal water bath; (4) gas mixer; (5) tubular reactor; (6) dring chamber; (7) GC-FPD; (8) data logger.

shrinkage of hydrogel to a large extent during the drying process at the ambient pressure and thereby losing the mesopores present in them. Fig. 2 also shows that the original microstructure of gel composite is maintained after H_2S breakthrough measurement, but the gel composite exhibits slightly denser network after desulphurization. The EDX spectra in Fig. 2e and f show that ZnO has been successfully introduced in the gel composites, and H_2S has been adsorbed onto the gel composites, suggesting that the as prepared materials can be used for H_2S removal.

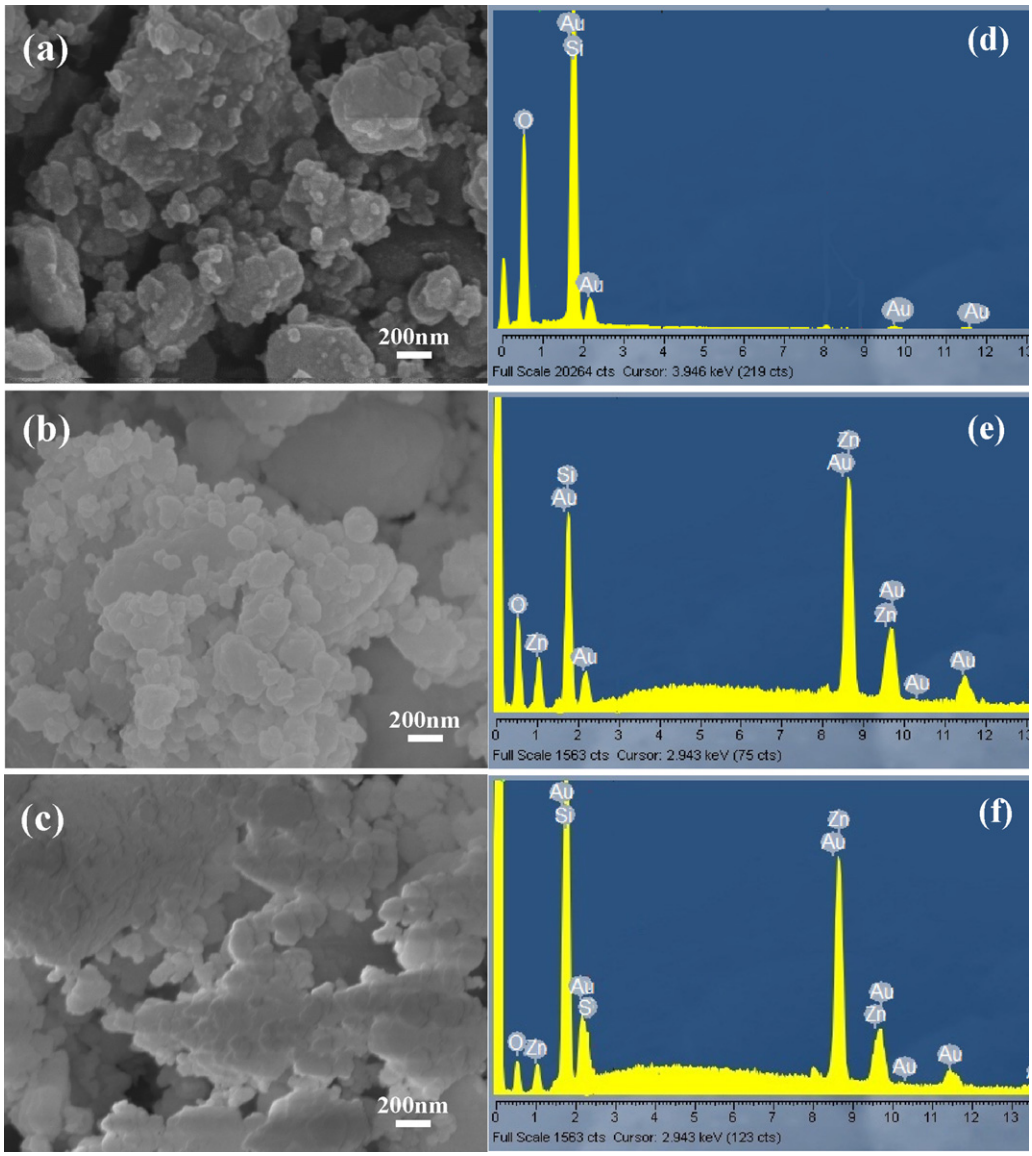

Fig. 2. SEM images of silica xerogel (a), ZnO/SiO_2 gel composite with 30 wt% ZnO treated at 400 °C before (b) and after (c) the desulphurization; EDX analysis of the region shown in (a), (b) and (c) corresponding to (d), (e) and (f), respectively; the Au peaks result from the conductive material coating.

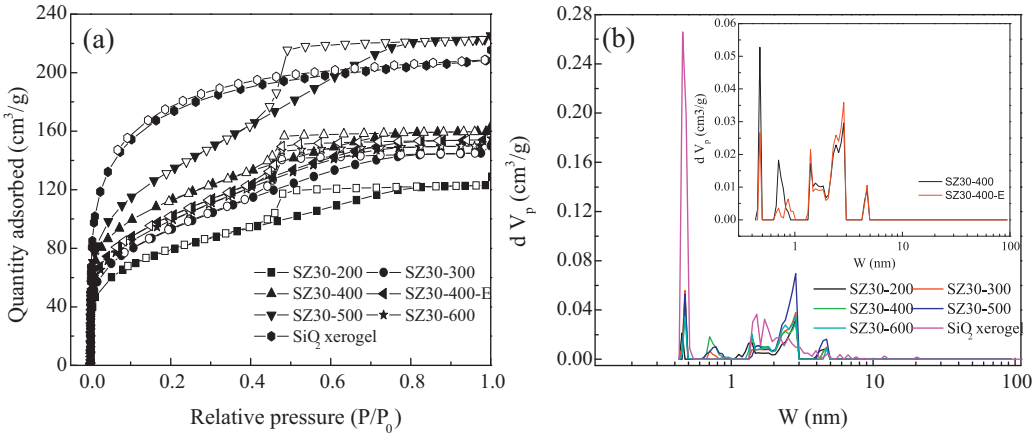

Fig. 3. Nitrogen adsorption–desorption isotherms (a) and PSDs calculated by DFT method (b) of samples. Insert: PSDs of gel composites before and after the desulphurization.

Fig. 3 shows the nitrogen adsorption–desorption isotherms and DFT pore size distributions of SiO_2 xerogel and ZnO/SiO_2 gel composites calcined at different temperature. The nitrogen adsorption–desorption isotherms and PSDs of the gel composites with different ZnO ratio are not shown here as they are similar to these series samples treated at different temperatures. The structural properties of all samples are shown in Table 1. For the SiO_2 xerogel, the isotherm is type I with a very small H2 type hysteresis loop in the IUPAC classification, indicating that the sample possesses a characteristic of microporous solids with very small mesopores [18]. This kind of isotherm could be either due to the presence of very narrow mesopores or to a bimodal distribution having one maximum in the micropore and another one in the mesopore range [19]. The isotherms of all ZnO/SiO_2 gel samples belong to a mixed type in the IUPAC classification. In their initial part they are type I, with an important uptake at low relative pressure. At intermediate and high relative pressures they are type IV with a hysteresis loop of type H2, which is normally associated with "ink-bottle" pores. With the increase of temperature up to 500 °C, the isotherms show a broader desorption plateau that might be due to a larger body/neck ratio than for the low temperature samples where less capillary condensation takes place [20]. Further increasing of temperature to 600 °C, the hysteresis loop become smaller, suggesting that the proportion of mesopores decreases, which may be attributed to the shrinkage and block of mesopores at higher treatment temperature.

Fig. 3b displays the PSDs obtained by applying the DFT method to N_2 adsorption data of prepared ZnO/SiO_2 gel composites and SiO_2 xerogel. All samples possessed roughly multimodal PSDs with distinct maxima in the micropore and small mesopore regions. The SiO_2 xerogel shows a sharp peak at about 0.5 nm, two broad peaks in the range 1–2 nm and small amount of mesopores in 2–5 nm. The ZnO/SiO_2 gel composites treated at different temperature show relative weak peaks around 0.5 nm, indicating the decrease of microporosity in these samples. The PSDs are widened by the increase of temperature up to 500 °C, with two significant peaks in the range of 2–3 nm and 4–5 nm respectively, and then the PSDs tend to be narrower by further rising of temperature. It suggests that the loading of ZnO and heat treatment lead to the widening of pore size and decrease of surface area, which is also proved by the textural parameters listed in Table 1. As seen from the table, the BET surface areas and the total pore volumes of the samples except SZ5-500 and SZ10-500, are lower than that of the pure SiO_2 xerogel, indicating that loading of the ZnO reduced the BET surface area and the pore volume of the original silica xerogel. It is worth to note that the SiO_2 xerogel was prepared by ambient drying at 80 °C. The unreacted precursor could not be pyrolysed, leading to somewhat blockage of the pores. For the ZnO/SiO_2 gel composites, which have been treated at high temperature, the unreacted precursor would be exhausted by pyrolysis process, and as a result, the samples with low ZnO ratio (5 and 10 wt%) exhibits higher surface area comparing to SiO_2 xerogel. However, further increase of ZnO ratio would lead to the decrease of surface area as observed for other samples, which is mainly attributed to the partial plugging of pore entrances and/or the pores by ZnO.

Fig. 3a also shows that the nitrogen uptake of SZ30-400-E decreases after the desulphurization, and the type of isotherm and

Table 1
Textural parameters of ZnO/SiO_2 gel composites prepared at different temperature.

Sample		ZnO ratio (wt%)	Treated temperature (°C)	S_{BET} (m^2/g)	V_t (cm^3/g)	W_a (nm)	Breakthrough time (min)	Breakthrough capacity (mg/g)
1	SiO_2 xerogel	0	–	612	0.32	2.11	1	0.8
2	SZ5-500	5	500	765	0.46	2.42	7	5.3
	SZ10-500	10	500	730	0.44	2.42	19	14.4
	SZ20-500	20	500	407	0.33	3.27	36	27.3
	SZ30-500	30	500	478	0.35	2.90	40	30.4
	SZ40-500	40	500	377	0.45	4.72	33	25.0
	SZ50-500	50	500	390	0.46	4.69	33	25.0
3	SZ30-200	30	200	282	0.19	2.72	5	3.8
	SZ30-300	30	300	335	0.23	2.72	60	45.5
	SZ30-400	30	400	399	0.25	2.48	127	96.4
	SZ30-500	30	500	478	0.35	2.90	40	30.4
	SZ30-600	30	600	357	0.24	2.65	4	3.0
4	SZ30-400-E	30	400	366	0.24	2.65	–	–

[*] S_{BET}: surface area calculated by BET method; V_t: total pore volume; W_a: average pore width.

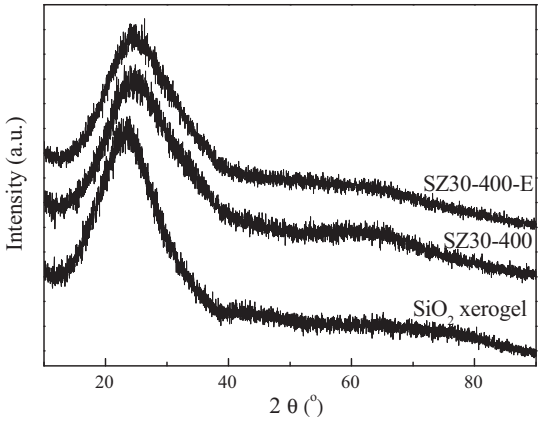

Fig. 4. XRD patterns of SiO_2 xerogel, ZnO/SiO_2 before and after the desulphurization.

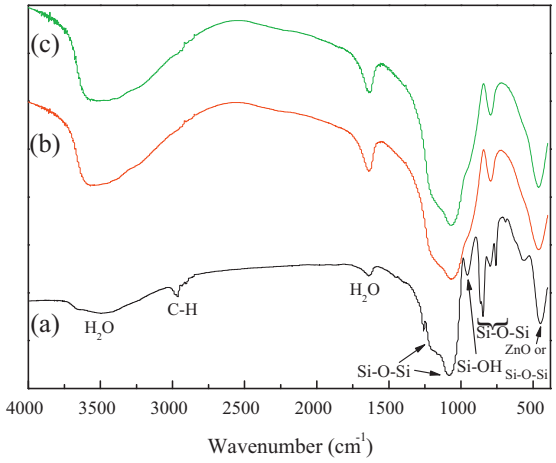

Fig. 5. FTIR spectra of SiO_2 xerogel (a), ZnO/SiO_2 gel composites before (b) and after (c) H_2S desulphurization.

hysteresis loop are still maintained, indicating that some pores are blocked during the removal of H_2S, but the porous structure is not affected. The inset in Fig. 3b shows that the intensity of pores centered at around 0.5 nm and 0.7 nm decreases significantly after the desulphurization, suggesting that the adsorption of H_2S mainly occurs in pores smaller than 1 nm. Therefore, it can be inferred that the ZnO particles are probably present in the mesopores of silica matrix and form several micropores. After the desulphurization reaction, some new products with larger volume are formed, which leads to the material expansion and partial collapse, and eventually pore volume and porosity reduction after desulfurization experiment. This is quite different from the results of desulphurization measurement on SBA-15 supported ZnO nanoparticles, for which the reaction mainly occurs on mesopores [8]. According to the previous studies [8,21–23], the desulphurization process of sorbents with ZnO as active component would follow this equation:

$$ZnO + H_2S \rightarrow ZnS + H_2O \quad (1)$$

Usually, ZnS is very stable under dry condition, but it would be oxidized to form $ZnSO_4$ when being exposed in atmosphere, especially in moist air, and this process could further decrease the surface area and pore volume, for which is mainly attributed to the blockage and thereafter leads to the decrease of micropores.

3.2. XRD analysis

Fig. 4 shows XRD pattern of SiO_2 xerogel, ZnO/SiO_2 gel composite prepared at 400 °C before and after the desulphurization. All samples exhibit typical amorphous structure. The peak of SZ30-400 around 2θ=25° shifts slightly towards small angle compared to SiO_2 xerogel, which is probably due to the modification of ZnO. However, there is no obvious diffraction peak corresponding to ZnO for SZ30-400, which may be attributed to the following reasons: the good dispersion of ZnO over SiO_2 xerogel [24], amorphous property of ZnO particles and/or the ZnO particles are smaller than the detection limits (ca. 5 nm) of the XRD method [25]. It suggests that in the amorphous ZnO/SiO_2 gel composites, finely divided amorphous ZnO particles are formed and stabilized by the porous texture of the formed SiO_2 xerogel, which hinders the movement and coalescence of ZnO particles. In addition, the XRD pattern of SZ30-400 shows little change after the desulphurization, indicating that there is not significant influence of product (ZnS) on the gel composite's structure.

3.3. FTIR analysis

The FTIR spectra of SiO_2 xerogel and ZnO/SiO_2 gel composites before and after desulphurization are shown in Fig. 5. It can be seen that there are several adsorption bands in the IR spectra of SiO_2 xerogel. The adsorption bands at 465, 798 and 1087 cm^{-1} correspond to different modes of silicon oxide: bending, symmetric and asymmetric, respectively [26], and the absorption band around 960 cm^{-1} is due to the stretching vibration of Si—OH [27]. The band at about 546 cm^{-1} is associated with double six-membered ring, which confirms the presence of microporous structure [8] in SiO_2 xerogel, agreeing with the N_2 adsorption–desorption isotherm. There are two H_2O adsorption peaks at 3440 and 1633 cm^{-1}, respectively. The broad adsorption peak at around 3440 cm^{-1} is assigned to the O—H asymmetrical stretching vibration of structural water; while the adsorption peak at around 1600 cm^{-1} is ascribed to the H—OH bending vibration of H_2O adsorbed in capillary pores and on the surface. The adsorption bands near 2981, 2933 and 2902 cm^{-1} are assigned to C—H stretching and deformation vibrations [28]. The other adsorption bands observed in the range of 1500–1350 cm^{-1} are due to the bending vibrations of C—H bonds [29].

The amount of adsorption bands in FTIR spectra of SZ30-400 decreases sharply comparing to SiO_2 xerogel, indicating that the types of functional groups decrease after the ZnO modification and heat treatment, and the surface of the sample tends to be more homogeneous. As seen in IR spectra of SiO_2 xerogel, the fairly sharp peak at 465 cm^{-1} is also observed for SZ30-400, and this peak also can be attributed to ZnO [8,13,30,31], which may be overlapped with O—Si—O. There is not remarkable change for the IR spectra of sample after desulphurization, and the peaks of sulfur-containing functional groups are not observed, which may be attributed to the overlap of ZnS by the absorbed peaks of Si—OH at around 960 cm^{-1} [32]. These results suggests that after the desulphurization process, the ZnO/SiO_2 gel composites still maintain the mesoporous features, and it may be helpful to the further use of these adsorbents.

3.4. Desulphurization performance

The H_2S breakthrough curves for various adsorbents are demonstrated in Fig. 6, and the breakthrough capacity of material obtained is summarized in Table 1. The breakthrough time measured for SiO_2 xerogel is very short (ca. 1 min) although it possesses a highest surface area, indicating that the xerogel is a poor adsorbent for H_2S. On the contrary, the breakthrough times of ZnO/SiO_2 gel composites are longer, indicating the better retention of H_2S on these materials compared to SiO_2 xerogel, and obviously, the H_2S concentration of outlet can be effectively controlled below 1 ppm before

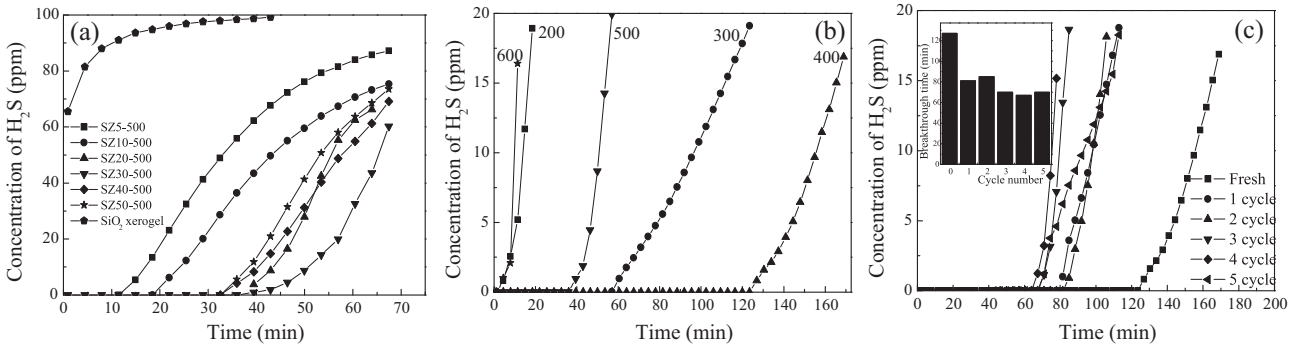

Fig. 6. H_2S breakthrough curves for ZnO/SiO_2 gel composites treated at 500 °C with different ZnO ratio (a), samples treated at different temperature with 30 wt% ZnO (b) and multiple H_2S adsorption/regeneration cycles for sample SZ-30-400 (c). Operation condition: 1 atm; 20 °C; inlet gas concentration: 100 ppm H_2S (balance of N_2); flow rate: 300 mL/min; mass of adsorbent: 0.06 g.

breakthrough. A commercial silica gel also shows very low H_2S adsorption capacity, and the capacity can be improved efficiently by the loading of triethanolamine (TEA) [33]. Not only silica gel, the synthesized mesoporous molecular sieve SBA-15 also shows poor sensitivity to H_2S, and the loading of polyethylenimine (PEI) can get a good breakthrough capacity [34]. These results suggest that silica gel or other similar materials can be used as good support for various active phases for the desulphurization, although they are very insensitive to H_2S.

Fig. 6a shows that the breakthrough time increases with the ZnO ratio up to 30 wt%, and decreases by further rising of the ZnO loading. It suggests that low ZnO loading results in low desulphurization efficiency, but excessively high ZnO ratio is also detrimental to the removal reaction. This is because that the ZnO aggregation possibility is increased by increasing the ZnO content, leading to a reduction of the active ZnO centers exposed for H_2S adsorption, while at lower ZnO content, a better dispersion of ZnO active centers can be achieved. As Fig. 6b shows, with the increase of treatment temperature, the breakthrough time of ZnO/SiO_2 composites first increases sharply up to 400 °C, and then decreases dramatically with further rising of temperature beyond 500 °C. The sample SZ30-400 exhibits a super affinity to H_2S and the breakthrough capacity is up to 96.4 mg/g. The results of nitrogen adsorption show that the porous structure of ZnO/SiO_2 composites is directly affected by calcination temperature. Unlike the surface area and pore volume, the average pore size (W_a) of the samples undergoes some oscillations, and SZ30-400 shows the lowest W_a. Fig. 3b also shows that the SZ30-400 and SZ30-600 possess the similar PSDs, which are narrower than other samples. Therefore, a narrower PSD would result in a higher H_2S removal capacity. However, the desulfurization performance does not depend on only one factor, and the yield of a desulfurization process directly depends on the physicochemical properties of the used adsorbent: porous texture, specific surface area and crystallite size of the active phase [35]. Table 1 shows that the trend of the enhancement in the adsorption capacity does not correlate to the increase of porosity. This is an indication that not only physisorption, but also chemical reaction governs H_2S removal process. As a result, the sample SZ30-600 shows much lower H_2S desulfurization capacity, although it has narrower PSD. Thus, the temperature would have significant influence on the structure of the gel composites not just reflected by the surface area and pore volume. In the current experiment, the treatment temperature of 400 °C may be a much suitable point for the well interaction between ZnO and SiO_2 to form cavities, in which a good match between the size of H_2S and the size of cavities is achieved.

Fig. 6c shows breakthrough curves for the gel composite SZ30-400 upon multiple H_2S adsorption/regeneration cycles, and the sample is regenerated at the calcination temperature of 400 °C for 3 h. It is shown that the sulfur capacity is different for each cycle, and at the 5th cycle, sulfur capacity is as high as 55% of its original value. This value is not very high, and may be due to the incomplete regeneration of the sample at 400 °C, which is the same condition as the sample preparation for the comparison of experimental results, but not high enough for the complete regeneration. However, it still indicates that the ZnO/SiO_2 gel composites are stable and show good performance in the removal of H_2S at low temperature.

In order to verify the mechanism of desulfurization on ZnO/SiO_2 gel composites, binding energy was measured by XPS on the gel composites before and after desulfurization, and the survey spectra of all elements and XPS spectra of $Zn2p_{3/2}$ and S2p are shown in Fig. 7. High-resolution XPS curves in the region of 1020–1025 eV are recorded, which shows two intense peaks at a binding energy (BE) of 1022.5 and 1021.8 eV for samples before and after desulphurization experiment, respectively. The former is a characteristic of the $2p_{3/2}$ transition of ZnO [21], indicating that ZnO is introduced in the composites as a component. Since the XRD analysis does not detect

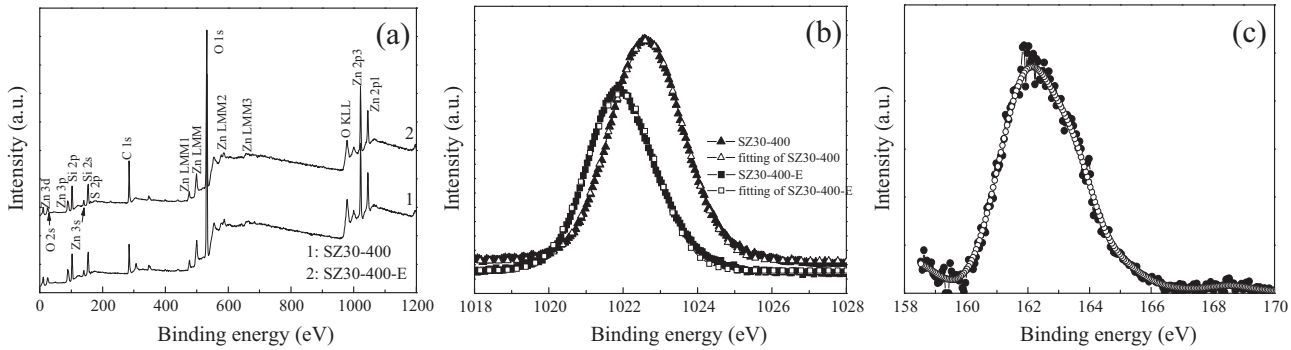

Fig. 7. XPS spectra of the whole spectra (a), Zn $2p_{3/2}$ (b) and S 2p (c) narrow spectra for ZnO/SiO_2 gel composites before and after desulphurization.

Table 2
Atomic concentration of ZnO/SiO_2 gel composites before and after desulphurization measured by XPS.

Sample	C1s	O1s	Si2p	S2p	Zn2p3
SZ30-400	24.49	46.48	22.98	0.02	6.03
SZ30-400-E	27.15	43.72	21.47	2.35	5.31

obvious diffraction peaks of ZnO, it is likely that ZnO has been well dispersed in the composites. The BE shift of $Zn2p_{3/2}$ from 1022.5 to 1021.8 eV after desulphurization experiment indicates that the chemical environment of Zn^{2+} has been changed, which is assigned to the conversion of ZnO to ZnS [21,22]. Fig. 7c shows that there is a BE peak at 162.1 eV, which is the characteristic of the S2p transition of sulfide [36]. XPS analysis for $S2p_{3/2}$ was also conducted to get further reaction information, and the presence of ZnS was detected at around 162 eV [22,23]. Therefore, the main product is ZnS in the process of desulphurization on ZnO/SiO_2 gel composites. The atomic concentration in Table 2 exhibits that the atomic concentration of S increases up to 2.35%, which indicates that H_2S has been adsorbed onto the gel composites, in agreement with the EDX analysis. Since both EDX and XPS only give the surface atomic percentage of materials, the current results suggest that the adsorption of H_2S not only occurs on the surface, but also in the bulk of the materials, which possess three dimensional porous structures.

4. Conclusions

High surface area ZnO/SiO_2 gel composites were successfully prepared by co-sol/gel method and ambient drying, followed by thermal treatment at different temperatures. The porous structure was significantly affected by ZnO ratio and treated temperature. The composites showed multimodal pore size distributions in micropore and mesopore region, and exhibited high H_2S removal capacities, in which the highest value is up to 96.4 mg/g for the sample treated at 400 °C with 30 wt% ZnO. Not only physisorption, but also the active phase reactivation governed the H_2S removal process, which occurred in both surface and bulk of the composites. It needs to optimize the composites' porous structure and active component loading amount.

Acknowledgement

The authors are grateful for the financial support from the National High Technology Research and Development Program of China (863 Program-no. 2010AA064907).

References

[1] R. He, F.-F. Xia, J. Wang, C.-L. Pan, C.-R. Fang, Characterization of adsorption removal of hydrogen sulfide by waste biocover soil, an alternative landfill cover, J. Hazard. Mater. 186 (2011) 773–778.
[2] D. Gabriel, M.A. Deshusses, Retrofitting existing chemical scrubbers to biotrickling filters for H_2S emission control, Proc. Natl. Acad. Sci. U.S.A. 100 (2003) 6308–6312.
[3] F. Adib, A. Bagreev, T.J. Bandosz, Analysis of the relationship between H_2S removal capacity and surface properties of unimpregnated activated carbons, Environ. Sci. Technol. 34 (2000) 686–692.
[4] A. Bagreev, J.A. Menendez, I. Dukhno, Y. Tarasenko, T.J. Bandosz, Bituminous coal-based activated carbons modified with nitrogen as adsorbents of hydrogen sulfide, Carbon 42 (2004) 469–476.
[5] D. Nguyen-Thanh, T.J. Bandosz, Activated carbons with metal containing bentonite binders as adsorbents of hydrogen sulfide, Carbon 43 (2005) 359–367.
[6] W. Michalak, E. Broitman, M.A. Alvin, A.J. Gellman, J.B. Miller, Interactions of SO_2 and H_2S with amorphous carbon films, Appl. Catal. A-Gen. 362 (2009) 8–13.
[7] D. Nguyen-Thanh, T.J. Bandosz, Effect of transition-metal cations on the adsorption of H_2S in modified pillared clays, J. Phys. Chem. B 107 (2003) 5812–5817.
[8] X.H. Wang, T.H. Sun, J. Yang, L. Zhao, J.P. Jia, Low-temperature H_2S removal from gas streams with SBA-15 supported ZnO nanoparticles, Chem. Eng. J. 142 (2008) 48–55.
[9] H.F. Garces, H.M. Galindo, L.J. Garces, J. Hunt, A. Morey, S.L. Suib, Low temperature H(2)S dry-desulfurization with zinc oxide, Microporous Mesoporous Mater. 127 (2010) 190–197.
[10] K. Polychronopoulou, J.L.G. Fierro, A.M. Efstathiou, Novel Zn–Ti-based mixed metal oxides for low-temperature adsorption of H_2S from industrial gas streams, Appl. Catal. B 57 (2005) 125–137.
[11] P. Dhage, A. Samokhvalov, D. Repala, E.C. Duin, B.J. Tatarchuk, Regenerable Fe-Mn-ZnO/SiO(2) sorbents for room temperature removal of H(2)S from fuel reformates: performance, active sites, operando studies, Phys. Chem. Chem. Phys. 13 (2011) 2179–2187.
[12] H. Yang, B. Tatarchuk, Novel-doped zinc oxide sorbents for low temperature regenerable desulfurization applications, AIChE J. 56 (2010) 2898–2904.
[13] X.H. Wang, J.P. Jia, L. Zhao, T.H. Sun, Chemisorption of hydrogen sulphide on zinc oxide modified aluminum-substituted SBA-15, Appl. Surf. Sci. 254 (2008) 5445–5451.
[14] L. Znaidi, Sol–gel-deposited ZnO thin films: a review, Mater. Sci. Eng. B-Adv. Funct. Solid-State Mater. 174 (2010) 18–30.
[15] J. Wang, Y. Qi, Z. Zhi, J. Guo, M. Li, Y. Zhang, A self-assembly mechanism for sol–gel derived ZnO thin films, Smart Mater. Struct. 16 (2007) 2673–2679.
[16] G. Buelna, Y.S. Lin, Characteristics and desulfurization-regeneration properties of sol–gel-derived copper oxide on alumina sorbents, Sep. Purif. Technol. 39 (2004) 167–179.
[17] S.A. Corr, Y.K. Gun'ko, A.P. Douvalis, M. Venkatesan, R.D. Gunning, P.D. Nellist, From nanocrystals to nanorods: new iron oxide-silica nanocomposites from metallorganic precursors, J. Phys. Chem. C 112 (2008) 1008–1018.
[18] K.S.W. Sing, D.H. Everett, R.A.W. Haul, L. Moscou, R.A. Pierotti, J. Rouquerol, T. Siemieniewska, Reporting physisorption data for gas solid systems with special reference to the determination of surface-area and porosity (recommendations 1984), Pure Appl. Chem. 57 (1985) 603–619.
[19] M. Casu, M.F. Casula, A. Corrias, G. Paschina, Textural characterization of high temperature silica aerogels, J. Non-Cryst. Solids 315 (2003) 97–106.
[20] R. Al-Oweini, H. El-Rassy, Surface characterization by nitrogen adsorption of silica aerogels synthesized from various Si(OR)(4) and RSi(OR')(3) precursors, Appl. Surf. Sci. 257 (2010) 276–281.
[21] S. Chaturvedi, J.A. Rodriguez, J. Hrbek, Reaction of S-2 with ZnO and Cu/ZnO surfaces: photoemission and molecular orbital studies, J. Phys. Chem. B 101 (1997) 10860–10869.
[22] J.A. Rodriguez, T. Jirsak, S. Chaturvedi, J. Hrbek, The interaction of H_2S and S-2 with Cs and Cs/ZnO surfaces: photoemission and molecular-orbital studies, Surf. Sci. 407 (1998) 171–188.
[23] L. Liu, R. Xie, L. Yang, D. Xiao, J. Zhu, Synthesis, structural, and optical properties of core/shell ZnS:Fe/ZnS nanocrystals, Phys. Status Solidi A-Appl. Mater. 208 (2011) 863–867.
[24] A. Auroux, A. Gervasini, C. Guimon, Acidic character of metal-loaded amorphous and crystalline silica-aluminas determined by XPS and adsorption calorimetry, J. Phys. Chem. B 103 (1999) 7195–7205.
[25] R.Z.L. Machala, A. Gedanken, Amorphous iron(III) oxides – a review, J. Phys. Chem. B 111 (2007) 4003–4018.
[26] B.E. Yoldas, Modification of polymer-gel structures, J. Non-Cryst. Solids 63 (1984) 145–154.
[27] A.V. Rao, P.B. Wagh, Preparation and characterisation of hydrophobic silica aerogels, Mater. Chem. Phys. 53 (1998) 13–18.
[28] J. Estella, J.C. Echeverria, M. Laguna, J.J. Garrido, Effects of aging and drying conditions on the structural and textural properties of silica gels, Microporous Mesoporous Mater. 102 (2007) 274–282.
[29] N. Hering, K. Schreiber, R. Riedel, O. Lichtenberger, J. Woltersdorf, Synthesis of polymeric precursors for the formation of nanocrystalline Ti–C–N/amorphous Si–C–N composites, Appl. Organomet. Chem. 15 (2001) 879–886.
[30] C. Wei, L. Fan, C. Yiwang, Y. Kai, C. Lie, Enhancement of the ultraviolet emission of ZnO nanorods by terphenyl liquid-crystalline ligands modification, Appl. Surf. Sci. 257 (2011).
[31] L. Zhang, M. Zhong, H. Ge, Surface modification of zinc oxide nanorods for potential applications in organic materials, Appl. Surf. Sci. 258 (2011) 1551–1554.
[32] H. Gunzler, H.U. Gremlich, IR Spectroscopy, Wiley-VCH, Weinheim, Germany, 2002.
[33] L. Zhou, L.M. Zhong, M. Yu, Y.P. Zhou, Sorption and desorption of a minor amount of H_2S on silica gel covered with a film of triethanolamine, Ind. Eng. Chem. Res. 43 (2004) 1765–1767.
[34] X. Wang, X. Ma, X. Xu, L. Sun, C. Song, Mesoporous-molecular-sieve-supported polymer sorbents for removing H(2)S from hydrogen gas streams, Top. Catal. 49 (2008) 108–117.
[35] R.L. Goswamee, F. Bosc, D. Cot, A. El Mansouri, M. Lopez, F. Morato, A. Ayral, Sol–gel derived nanocomposites and nanoporous oxide powders and related coatings for the reversible chemisorption of hydrogen sulfide, J. Sol–Gel Sci. Technol. 29 (2004) 97–105.
[36] J.F. Moulder, W.F. Stickle, P.E. Sobol, K.D. Bomben, Handbook of X-ray Photoelectron Spectroscopy, Perkin-Elmer Corporation, Eden Prairie, Minnesota, 1992.